Transient-based frequency domain method for dead-end side branch detection in reservoir-pipeline-valve systems

HF Duan[1], *M.ASCE*; and PJ Lee[2], *M.ASCE*

[1] *Assistant Professor, Department of Civil and Environmental Engineering, The Hong Kong Polytechnic University, Hung Hom, Kowloon, SAR Hong Kong, China. (Corresponding Author) Email: hf.duan@polyu.edu.hk.*

[2] *Senior Lecturer, Department of Civil and Natural Resources Engineering, The University of Canterbury, Private Bag 4800 Christchurch, New Zealand. Email: pedro.lee@canterbury.ac.nz.*

Abstract: Unexpected, unknown or unused side pipe branches, termed dead-end side branches in this study, commonly exist in water pipe systems due to incorrect device installations or illegal connections. These connections are detrimental to the water quality as well as the operation and management of pipe networks. This paper investigates a transient-based frequency domain method for detecting side branches in pipe systems. The frequency response function for a pipe system with a single dead-end side branch is first derived by the transfer matrix method and the side branch was found to cause shifts in the system resonant frequencies. The nature of the resonant frequency shifts can be used to inversely determine the location and size of the side branch. A two-step Genetic algorithm based optimization is proposed in this study to efficiently solve the derived analytical expression for the resonant frequency shifts. The developed method is validated through numerical simulations and the results demonstrate the feasibility of this method for detecting side branches. The accuracy for locating the side branch is higher than the accuracy in sizing the branches. The sensitivity of the method to the magnitude and bandwidth of the transient wave signal is also discussed in the paper.

Keywords: Water pipe system; dead-end side branch; transient-based frequency domain method; transients; transfer matrix; genetic algorithm

Introduction

Urban water pipe systems support the water supply, drainage, sewage as well as sea water systems of cities and are central to the social, economic and health sectors. The understanding and monitoring of such pipe systems are crucial to their management and efficient operation. Unexpected dead-end side branches commonly exist in pipe networks because of careless pipe installation, historical system modifications resulting in orphan pipes and illegal connections (Stephens 2008; and Meniconi et al. 2011a). At times, severe blockages and accidentally shut isolation valves can also lead to the formation of such side branches. These pipe branches are normally hidden underground and the fluid in these branches is static or under very small flowrate such that they are hard to detect using steady-state based methods. In this study, the flow is assumed to be static within these branches.

It is important to locate these side branches as the stagnant water within can compromise the water quality across the networks and the impedance of the branches can affect the hydraulics responses of the networks under normal operations (Carter et al. 1997). Pressure surges from normal pump and valve operations can enter the side branch and the reflection at the termination end can magnify the wave front, creating pressure fluctuations in the pipe networks that exceed the original transient design capacity (Karney and McInnis 1990; and Ferrante et al. 2009). Currently the methods used for side branch detection are physical inspection and steady hydraulics based analysis (Walski et al. 2003; Meniconi et al. 2011a). Such methods are limited to short range or long duration tests that require many months to complete the survey of the system.

Due to the magnification of the transient signal at a side branch, a logical approach is to use small amplitude (e.g., 1 to 10 m in pressure head), controlled fluid transients as a means of

51 detecting these hidden pipe sections (Meniconi et al. 2011b). An advantage of this approach is
52 that fluid transient waves in elastic pipes travel at speeds exceeding 1000 m/s, allowing rapid
53 detection procedures. Transient-based method has been applied to the detection of leaks and
54 blockages in pipelines with good success (Liggett and Chen 1994; Brunone 1999; Vítkovský et
55 al. 2000, 2007; Wang et al. 2002, 2005a; Beck et al. 2005; Covas et al. 2005; Lee et al. 2006,
56 2008; Mohapatra et al. 2006; Ferrante et al. 2007; AL-Khomairi 2008; Kim 2008; Sattar et al.
57 2008; Stephens 2008; Tuck et al. 2013; Duan et al. 2011, 2012a, 2012b, 2013, 2014; Meniconi et
58 al. 2011a, 2011b, 2011c, 2013; and Kim et al. 2014). The principle of the transient based
59 diagnostic method is: (1) to induce a small amplitude pressure signal (2) to measure the
60 responses at accessible points in the system (such as hydrant points or maintenance locations)
61 and (3) to compare the data with analytical models, in order to inversely determine the size and
62 location of faults either in the time, or frequency domains (Colombo et al. 2009). It has been
63 shown in the literature that transient fault diagnostics in the frequency domain can allow the fault
64 to be isolated from complex system phenomena such as unsteady friction and pipe wall visco-
65 elasticity as well as providing an increased tolerance to random noises (Lee et al. 2006, and Duan
66 et al. 2011, 2012a). Therefore, in this study, the transient frequency responses of pipeline
67 systems are used to detect side braches.
68 Wang et al. (2005b) investigated the effect of lateral dead ends on the pipeline transients
69 by forward analysis, where a linear analytical solution in the form of a Fourier series was derived
70 for the shifting of harmonic frequencies by the lateral dead ends. Their results demonstrated the
71 significant impact of lateral dead ends on the resonant frequencies, which is a function of the
72 location, volume, and wave speed of the dead end. However, this study had a number of
73 limitations. The linear assumptions of small amplitude transients and dead-ends were adopted in

74 their study and the lumped volume of the potential dead end was used in the derivation such that
75 it is difficult to obtain the individual influence of the size and length of the dead ends on the pipe
76 transients respectively. Moreover, their study did not produce a method for the detection of
77 lateral dead ends in pipe systems.

78 A recent study by Meniconi et al. (2011a) has demonstrated the detection of inactive pipe
79 side branches using time domain techniques. The location of the illegal side branch is given by
80 the arrival time of the reflection from the branch, while the size of the side branch is determined
81 by a simple frictionless relationship with the size of the reflection. While this technique is shown
82 to work well, the number of reflections in a complex network can quickly become overwhelming
83 and the size of the branch may be underestimated using the frictionless approximation of the
84 system.

85 This paper presents a new frequency domain method for detecting side branches in pipe
86 systems. The impact of a side branch on the transient response of a pipeline is first presented to
87 illustrate how the response may be used for the detection and location of the branch. The impact
88 of the side branch on the system frequency response is derived analytically using the transfer
89 matrix method (Lee et al. 2006; Duan et al. 2011, 2012a), which is then used in a two-stage
90 inverse calibration method to show the accurate detection and location of the side branch. The
91 methodology is validated using numerical data simulated by the one-dimensional (1D) transient
92 method of characteristics model.

93

94 **1D water hammer models**

95 The classical 1D water hammer model is adopted in this study for analytical and numerical
96 investigations, mathematically expressed as (Chaudhry 1987; Wylie et al. 1993; and Ghidaoui et

97 al. 2005)

98 $$\frac{gA}{a^2}\frac{\partial H}{\partial t}+\frac{\partial Q}{\partial x}=0, \quad (1)$$

99 $$\frac{\partial Q}{\partial t}+gA\frac{\partial H}{\partial x}+\frac{\pi D}{\rho}\tau_w=0, \quad (2)$$

100 where H = pressure head, Q = pipe discharge, A = pipe cross-sectional area, D = pipe diameter, a
101 = wavespeed, t = time, x = spatial coordinate along pipeline, g = gravitational acceleration, ρ =
102 fluid density, and τ_w = pipe wall shear stress, and $\tau_w=\frac{\rho f}{8}V^2$, in which, V = pipe cross-sectional
103 area averaged velocity; $f = f_s + f_u$ = pipe friction factor, and f_s, f_u = steady and unsteady
104 components of pipe friction factor. Particularly, for laminar flow, $f_s = 64/\mathbf{Re}$ with $\mathbf{Re} = VD/\nu$ =
105 Reynolds number and ν = kinematic viscosity of water; while for turbulent flow f_s is determined
106 approximately by the Colebrook equation (e.g., Chaudhry 1987; Wylie et al. 1993)
107
108 **Importance of side branches to the transient modeling and analysis**
109 It has been widely evidenced in the literature that the side branches may have intense effect on
110 the transient responses of pipelines systems (e.g., Chaudhary 1987; Wylie et al. 1993). To clearly
111 demonstrate this effect in present study, the simple pipe system with a single side branch shown
112 in Fig. 1 is used for this example. The main pipeline (pipe sections no. 1 and no. 2) is bounded
113 by two constant head tanks (N_1 and N_2 in the figure) and the discharge in the pipeline is
114 controlled by the valve located at the downstream tank (N_2). A side branch is located at the
115 junction N_3 with zero discharge with the valve at terminal N_4 fully shut under the steady state
116 condition. The parameters of the system are as follows: (1) length (l): 400 m, 600 m, and 50 m;
117 (2) diameter (D): 0.6m, 0.5m, and 0.2m; and (3) wave speed (a): 1000 m/s, 1200 m/s, and 1300

118 m/s, for pipe sections no. 1, no. 2, and no. 3, respectively. The steady state discharge (Q_0) in the
119 main pipeline (pipe sections 1 and 2) is assumed to be 0.2 m^3/s.
120
121 [**Figure 1** will be here]
122
123 The transient is generated by the sudden closure of the downstream end valve at N_2.
124 Based on the 1D numerical models in Eqs. (1) through (3), the transient pressure heads in the
125 time domain at N_2 for a pipeline system without the side branch (pipe no. 3) and with the side
126 branch are plotted in Fig. 2(a) for comparison. Note that the grid size of the discretization is
127 fixed at 1 m for all pipe sections and spatial interpolation is applied in the numerical simulation
128 (Chaudhry 1987). The results show that the existence of the side branch could increase the
129 magnitudes of the system transient responses in certain locations in the system (e.g., the location
130 N_2 shown here). These increases in the transient response may exceed the designed capacity of
131 the pipe system.
132 Furthermore, the side branch has induced more wave oscillations by creating reflections
133 in the transient responses, which can affect the dynamics of air-chambers, surge tanks and air-
134 valves in the system (Duan et al. 2010a). The increased pressure oscillations are confirmed by
135 the frequency domain results in Fig. 2(b), which demonstrates the shifting of resonant peaks and
136 energy transfers between different frequency modes (amplitude changes). Note that current
137 transient-based pipe leakage/blockage detection methods rely on the reflection and damping
138 information of the measured/simulated transient responses (Duan et al. 2010b), therefore the
139 understanding and characterization of the impact of side branches on transient reflections and
140 damping is important for system design (modeling and analysis) as well as system management

141 (pipe defects detection). This paper aims to characterize the transient behavior of dead-end side
142 branches in the pipe system and develop a transient-based frequency domain method for the side
143 branch detection.
144
145 [**Figure 2** will be here]
146
147 **Analytical results of frequency responses for pipe systems with a side branch**
148 To derive the frequency responses, the 1D mass and momentum equations in Eqns. (1) and (2)
149 are first linearized and transformed into frequency domain equivalents to describe the behaviors
150 of the transient pipe system (Chaudhry 1987; Duan et al. 2011, 2012a). The result of the
151 downstream transient responses in terms of the upstream quantities can be obtained as (Lee et al.
152 2006),

153 $$\begin{Bmatrix} q \\ h \end{Bmatrix}^{n+1} = \begin{bmatrix} \cos(\mu l) & i\frac{1}{Y}\sin(\mu l) \\ iY\sin(\mu l) & \cos(\mu l) \end{bmatrix} \begin{Bmatrix} q \\ h \end{Bmatrix}^{n}, \tag{3}$$

154 where $\mu = C_R \frac{\omega}{a}$ = wave number; $Y = -C_R \frac{a}{gA}$ = characteristic impedance; $C_R = \sqrt{1 - i\frac{gAR}{\omega}}$ =
155 friction coefficient; $R = \frac{fQ}{gDA^2}$ = friction damping factor; q, h = discharge and pressure head in
156 the frequency domain; n, n+1 = upstream and downstream ends of pipe section; ω = frequency;
157 and i = imaginary unit. The expression for friction damping factor R, derived in Vítkovský et al.
158 (2003) is used in this study. Note that this friction damping factor includes the effect of unsteady
159 friction.
160 The transient frequency response function is a fundamental description of the system
161 behavior and this function has been applied for the detection of leaks (Lee et al. 2006; Duan et al.

2011), blockages (Mohapatra et al. 2006; Lee et al. 2008; Sattar et al. 2008; Duan et al. 2012a, 2013, 2014), and the description of pipe wall visco-elasticity (Duan et al. 2012b). Using similar procedures in these studies, the transient frequency responses are derived for side branches in this paper. Using the system configuration of Fig. 1, the transient frequency response function at the valve N_2 is obtained as (see Eq. 10 in the appendix),

$$h^{N_2} = i\frac{\begin{array}{l} Y_2Y_3\cos(\mu_3 l_3)\sin(\mu_2 l_2)\cos(\mu_1 l_1) - Y_2Y_1\sin(\mu_3 l_3)\sin(\mu_2 l_2)\sin(\mu_1 l_1) \\ +Y_1Y_3\cos(\mu_3 l_3)\cos(\mu_2 l_2)\sin(\mu_1 l_1) \end{array}}{\begin{array}{l} Y_1Y_3\cos(\mu_3 l_3)\sin(\mu_2 l_2)\sin(\mu_1 l_1) + Y_1Y_2\sin(\mu_3 l_3)\cos(\mu_2 l_2)\sin(\mu_1 l_1) \\ -Y_2Y_3\cos(\mu_3 l_3)\cos(\mu_2 l_2)\cos(\mu_1 l_1) \end{array}}. \quad (4)$$

Detailed derivations are presented in the appendix. The resonant condition for the single side branch system is given by Eq. (13) in the appendix,

$$\begin{bmatrix} Y_2Y_1\sin(\mu_3 l_3)\cos(\mu_2 l_2)\sin(\mu_1 l_1) \\ -Y_3Y_2\cos(\mu_3 l_3)\cos(\mu_2 l_2)\cos(\mu_1 l_1) \\ +Y_3Y_1\cos(\mu_3 l_3)\sin(\mu_2 l_2)\sin(\mu_1 l_1) \end{bmatrix} = 0, \quad (5)$$

or alternatively,

$$\begin{bmatrix} (Y_2Y_3 + Y_1Y_2 + Y_1Y_3)\cos(\mu_1 l_1 + \mu_2 l_2 + \mu_3 l_3) \\ +(Y_2Y_3 - Y_1Y_2 - Y_1Y_3)\cos(\mu_1 l_1 - \mu_2 l_2 - \mu_3 l_3) \\ +(Y_2Y_3 + Y_1Y_3 - Y_1Y_2)\cos(\mu_1 l_1 + \mu_2 l_2 - \mu_3 l_3) \\ +(Y_2Y_3 - Y_1Y_3 + Y_1Y_2)\cos(\mu_1 l_1 - \mu_2 l_2 + \mu_3 l_3) \end{bmatrix} = 0. \quad (6)$$

Note that in this study only the case of a single dead-end side branch is investigated and tested, and similar derivation process can be applied for the situations of multiple side branches in complex pipe system.

Simplification and analysis of analytical results

To use Eq. (5) for side branch detection, the resonant frequencies of the system have to be obtained by experimental measurement or numerical simulations, and then inversely fitted to Eq.

(5). To obtain the solution, an inverse method such as GA-based optimization used in Duan et al. (2012a) is needed. However, Eq. (5) is too implicit to show the direct relationship between the resonant frequencies and properties of the side branch. It is useful to further simplify the equation to obtain a clear illustration of this dependency, in a similar analytical procedure used for extended blockages in Duan et al. (2013, 2014). Under the assumption that the side branch is small relative to the main pipeline and using a first-order approximation, the simplified expression for the resonant frequency shifts by the side branch can be obtained as,

$$\frac{\Delta\omega_{rf}}{\omega_{th0}} = -\frac{2\varepsilon}{\pi}\frac{\sin\left[\lambda_3\omega_{rf0}\right]\cos^2\left[\lambda_2\omega_{rf0}\right]}{\cos\left[\lambda_3\omega_{rf0}\right]}, \tag{7}$$

where $\Delta\omega_{rf}=\Delta\omega_{rf}(k)$ = resonant frequency shift; $\omega_{rf0} = \omega_{rf0}(k)$ =system resonant frequency with subscript 0 indicating the system without a side branch; k = resonant peak number; $\omega_{th0} = \frac{\pi}{2\lambda_0} =$ theoretical (first resonance) frequency of the reservoir-pipe-valve system, that is, $\omega_{th0} = \omega_{rf0}(k=1)$; $\lambda = \mu l/\omega$ = wave propagation operator; and $\varepsilon = Y_0/Y_3$ = the ratio of characteristic impedances of main pipeline and side branch, and $\varepsilon << 1$ is assumed in the derivation of Eq. (7). Note that for simplification the resonant frequency peak number has been neglected in Eq. (7), but this equation is valid for all resonant peaks in the frequency domain.

Eq. (7) clearly shows the dependence of resonant frequency shifts on the side branch properties (i.e., branch size, length and location derived from the parameters ε, λ_3, and λ_2 respectively). Meanwhile, compared to the full form of Eq. (5), the simplified Eq. (7) is simpler to solve using the inverse fitting process. The solution of Eq. (7), however, could only provide a reasonable initial guess for solving the full form Eq. (5) due to the assumption of small side branch and linearity.

201

202 **Application procedure of side branch detection**

203 For accuracy, Eq. (5) has to be used to identify and obtain the properties of the side branch in the
204 system. The difficulty and complexity for solving Eq. (5) is very similar to that for the equation
205 of extended blockage detection in Duan et al. (2012a). Therefore, the genetic algorithm (GA)-
206 based optimization procedure adopted in Duan et al. (2012a) is also used herein for solving Eq.
207 (5). The objective function for the optimization is the absolute value of the left hand side of Eq.
208 (5), which will be minimized to close to zero as much as possible. To avoid singularity problems
209 during the optimization process, the variables are chosen as D_3, l_2, l_3, and a_2, instead of Y_3, λ_3,
210 and λ_2 in Eq. (5). The rewritten form of Eq. (5) is given by Eq. (14) in the appendix.

211 The efficiency and accuracy of the GA-based optimization is highly dependent on the
212 initial values and the search range. In this study, a two-step method is used, where Eq. (7) is first
213 solved to provide the initial values and searching ranges of all parameters for the GA-based
214 optimization of Eq. (5). It is assumed that the side branch is smaller than the main pipeline and
215 the search range of the size and length of the side branch range between zero to the values of the
216 main pipeline (that is $[0, \max(D_1, D_2)]$ and $[0, l_0]$ with $l_0 = l_1 + l_2$ as in Fig. 1).

217

218 [**Figure 3** will be here]

219

220 The GA scheme developed in Vítkovský et al. (2000) is used for the optimization. The
221 procedure of the GA-based optimization is shown in Fig. 3. The optimization process ends when
222 either one of the two conditions are met (1) the relative error of all the results for any two
223 continuous iterations is smaller than 1%; (2) the maximum iteration number, M = 5000, is

reached.

Numerical applications

Numerical tests are used to examine the two-step optimization procedure for detecting side branches. The test settings are listed in Table 1, covering a wide range of system scales and flow regimes. Ten numerical tests were conducted in this study to investigate the influence of different side branch configurations and hydraulic conditions on the accuracy of the proposed method. The total length of pipeline (l_0) without a side branch is kept at 1000 m, while the length, size and wavespeed of each pipe section divided by the side branch change with different tests. Smooth pipe friction factors are assumed for all pipe sections. Numerical transient simulations are conducted by the 1D water hammer equations coupled with unsteady friction models. The quasi-steady friction effect is represented by the Darcy-Weisbach formula; and the unsteady friction is calculated by Zielke's model for laminar flows (Zielke, 1968) and modeled by Vardy-Brown's model for turbulent flows (Vardy and Brown, 1995).

[**Table 1** will be here]

Transients in the system are caused by the operation of a side-discharge valve at point N_2 in Fig. 1. The discharge perturbation (Q_V) consists of a fast close-open-close operation of the valve as shown in Fig. 4, in order to generate a sharp wave signal with a large bandwidth in the system (Duan et al. 2010b, Lee et al. 2014). The influence of different input signals is discussed later in the paper. In Fig. 4, the valve discharge perturbation on the vertical coordinate is normalized by the initial steady state flowrate (Q_0) , and the axial time coordinate is normalized

by the wave period for the main pipeline ($4l_0/a_0$). The pressure head at point N_2 in Fig. 1 is collected for analysis.

[**Figure 4** will be here]

The simulated pressure head for test case no. 1 is plotted in Fig. 5 (a), where the vertical coordinate is the transient pressure head (ΔH_t) normalized by the *Joukowsky* head rise (i.e., $\Delta H_0 = a\Delta V_{v0}/g$ with ΔV_{v0} = the flow velocity change of the initial side discharge valve operation) and the axial coordinate is dimensionless time in terms of the wave period of the main pipeline. The frequency response function (Lee et al. 2006) is shown in Fig. 5 (b) with the vertical coordinate normalized by fundamental harmonic response of the main pipeline and the axial coordinate normalized by the fundamental frequency ($a/4l_0$) of main pipeline. For comparison, the results for a system without a side branch are also plotted in Fig. 5. The results demonstrate clearly the additional wave reflections in the time domain in Fig. 5(a) and the frequency shifts of resonant peaks in the frequency domain in Fig. 5(b).

[**Figure 5** will be here]

Results analysis and discussion

The results of Fig. 5 for test no. 1 are first used to illustrate the efficiency of two different optimization approaches for side branch detection: (1) inverse fitting the results directly to Eq. (5); and (2) using the two-step procedure shown in Fig. 3 to first inversely fit the results to the simplified Eq. (7) to provide a starting guess and refine the search space for a second inverse

optimization with Eq. (5). The first 15 resonant peaks in Fig. 5(b) are extracted for analysis. The operations of the two optimization schemes are shown in Fig. 6, which clearly indicates a faster convergence for the two-step optimization scheme. The CPU computation time for the two-step method is less than 1/3 of that for the direct GA-based optimization scheme for the same accuracy. Particularly in this test case here, the computation time required by two-step method is about 3 minutes, while that by direct optimization method is over 10 minutes.

[**Figure 6** will be here]

The result of the optimization for test no. 1 is plotted in Fig. 7, which reveals the good agreement between the results from the two-step optimization and the numerical data. Meanwhile, the result of Fig. 7 also shows clearly the improvement of the proposed two-step optimization compared to the single step optimization for Eq. (7) only. The two-step GA-based optimization scheme in Fig. 3 is used for side branch detection in the following analysis.

[**Figure 7** will be here]

The side branch characteristics determined for all the ten tests in Table 1 are shown in Table 2. The relative error of the prediction (γ in Table 2) for each parameter is given by,

$$\gamma_P(\%) = \frac{\left|P_r - P_p\right|}{P_r} \times 100\,, \tag{8}$$

where P is the parameter being considered and subscripts "r" and "p" refer to the real and predicted parameter values respectively. It is also necessary to point out that the predicted values

293 during the GA-based optimization process are real numbers with more than 3 decimal places, but
294 only the rounded integer values are shown here in Table 2.
295
296 [**Table 2** will be here]
297
298 The results in Table 2 demonstrate that the proposed approach can be applied for side
299 branch detection, as the prediction errors are within 20% for all parameters in the numerical tests
300 in this study. The maximum relative errors for D_3, l_3, a_3, and l_2 are 14.7%, 14.0%, 4.6% and
301 3.7% respectively (numbers in bold in Table 2), which implies that the proposed method is more
302 accurate for locating (l_2) than sizing (size D_3 and length l_3) the side branch. In addition, Table 2
303 indicates that the accuracy of the method is decreasing with the scales of the side branch under
304 the same other conditions during the testing (e.g., tests no. 3, 5 & 6; and tests no. 7 & 8), with the
305 worst prediction for test no. 3, which has the largest side branch amongst all the cases considered.
306 This large error is due to the violation of the small side branch approximation used in the
307 analytical derivation (e.g., $\varepsilon \leq 10\%$, $l_3/l_0 < 10\%$). Furthermore, the results in Table 2 also reveal
308 that detection accuracy under laminar flow (test no. 1 in Table 1) is higher than that for the
309 turbulent system (tests no. 2 through 10). For all the turbulent flow cases (tests no. 2 through 10),
310 the accuracy of the detection results is by and large decreasing with initial turbulent conditions
311 (i.e., $\boldsymbol{Re}_0$). This variation trend of the detection accuracy is mainly because of the linearization
312 approximation of the quasi-steady friction term (relatively small transient flow to the steady base
313 flow) used in the analytical derivation of Eq. (5) (Duan et al. 2013; and Meniconi et al. 2013). It
314 is necessary to note that this conclusion will require further systematical analysis and
315 experimental validations under a wide range of system configurations and conditions in the

316 future work.

317

318 **Influence of input transient signals**

319 For the practical application of the proposed method, it is also necessary to consider the impact
320 of different transient signals on the detection accuracy. Real valves will generate signals of
321 different properties and the sensitivity of the method to the shape of the signal is an important
322 consideration. Test no. 1 in Table 1 is used for this analysis and three different input signals
323 shown in Fig. 8 are used in conjunction with the proposed side branch detection method. In Fig.
324 8, signal #1 represents the "fast and sharp" (large frequency bandwidth) signal; while signal #2
325 represent a larger magnitude input signal but of the same shape and signal #3 is a signal of the
326 same magnitude as the original signal but of a much smoother form (small frequency bandwidth).

327

328 [**Figure 8** will be here]

329

330 For a fair comparison, only the first 7 resonant frequency peaks are used for side branch
331 detection as signal #3 do not have detectable resonant peaks beyond this point. The detection
332 results for the three different input signals are shown in Table 3, with the detection accuracies for
333 signals #2 and #3 being much lower than that for signal #1. This result implies that a small
334 amplitude but sharp signal produces the best accuracy from the method. This result is consistent
335 with previous studies in Duan et al. (2010b) and Lee et al. (2014). The larger errors with the
336 other signals are caused by the violation of the linearization approximation used in the analytical
337 derivation of Eq. (5) in the case for signal #2 (Lee and Vítkovský 2010) and the inaccurate
338 representation of high frequency resonant peaks (Lee et al. 2014) in the case for signal #3.

339

340 [**Table 3** will be here]

341

342 Furthermore, the results in Table 3 show that the influence of the input signal is more
343 profound for the prediction of the side branch size and length than for the side branch location
344 and wave speed. This result is consistent with the results and findings in previous studies for the
345 extended blockage detection (Duan et al. 2012a, 2013; and Meniconi et al. 2013), and is due to
346 the insensitivity of the resonant frequency to the size and length of the faults (e.g., side branch
347 and extended blockage) (Duan et al. 2014).

348

349 **Summary and conclusions**

350 This paper investigates the detection of dead-end side branch in pipe systems by using transient-
351 based frequency domain method. The transient responses for systems with and without side
352 branches are compared in this study to illustrate the need to identify such side branches in the
353 pipe system. Based on the transfer matrix method, the analytical expression of the frequency
354 response function for a single dead-end side branch in the pipe system is derived and used for the
355 detection of dead-end side branches in this study. The derived implicit equation is further
356 simplified based on the assumptions of small side branches and linearity, in order to give a clear
357 relationship between the resonant frequency shifts and the side branch information. This
358 simplified expression improves the initial guesses and search space for the genetic algorithm
359 (GA) based optimization. For this purpose, a two-step GA-based optimization scheme is
360 proposed in this study to provide a more efficient solution.

361 The developed dead-end side branch detection scheme has been validated by numerical

simulations in this study. The results show that the developed method coupled with the optimization scheme can provide an accurate detection of the side branches in pipe system. It is also found that the proposed two-step optimization scheme is more efficient than the common direct GA-based optimization method. At the same time, the results indicate that the developed method in this study can provide a more accurate prediction for the location and wavespeed of the dead-end side branches than that for the size and length of the branches. It is also noted that further experimental tests will be needed to test the robustness and accuracy of the proposed method for the detection of multiple side branches, and more investigations will be required to examine the influences of other practical complexities and factors such as fluid-structure interaction (FSI) and system uncertainties to the proposed method.

Acknowledgements

This research is supported by the research grants of the Hong Kong Polytechnic University (HKPU) under projects 1-ZVCD, G-UC73 and G-YBC9, and the Royal Society of New Zealand, Marsden Grant UOC-M1153.

Appendix: analytical derivation of transient frequency responses for pipe systems with dean-end side branches

Based on the method of transfer matrix in Eq. (3), the frequency responses at downstream end "N_2" in the system of Fig. 1 can be expressed as,

$$\begin{Bmatrix} q \\ h \end{Bmatrix}^{N_2} = \begin{bmatrix} \cos(\mu_2 l_2) & i\frac{1}{Y_2}\sin(\mu_2 l_2) \\ iY_2 \sin(\mu_2 l_2) & \cos(\mu_2 l_2) \end{bmatrix} \begin{bmatrix} 1 & Z_{DESB} \\ 0 & 1 \end{bmatrix} \begin{bmatrix} \cos(\mu_1 l_1) & i\frac{1}{Y_1}\sin(\mu_1 l_1) \\ iY_1 \sin(\mu_1 l_1) & \cos(\mu_1 l_1) \end{bmatrix} \begin{Bmatrix} q \\ h \end{Bmatrix}^{N_1}, \quad (9)$$

where Z_{DESB} = the hydraulic impendences of the dead-end side branch in the system of Fig. 1. After mathematical manipulation and rearrangement, the perturbations of transient pressure head at downstream *B* can be obtained as,

$$h^{N_2} = -\frac{iY_2 \sin(\mu_2 l_2)\cos(\mu_1 l_1) - Z_{DESB} Y_2 Y_1 \sin(\mu_2 l_2)\sin(\mu_1 l_1) + iY_1 \cos(\mu_2 l_2)\sin(\mu_1 l_1)}{\cos(\mu_2 l_2)\cos(\mu_1 l_1) - \frac{Y_1}{Y_2}\sin(\mu_2 l_2)\sin(\mu_1 l_1) + iY_1 Z_{DESB}\cos(\mu_2 l_2)\sin(\mu_1 l_1)}. \quad (10)$$

Therefore, the resonant condition for the branched pipe system is,

$$\cos(\mu_2 l_2)\cos(\mu_1 l_1) - \frac{Y_1}{Y_2}\sin(\mu_2 l_2)\sin(\mu_1 l_1) + iY_1 Z_{DESB}\cos(\mu_2 l_2)\sin(\mu_1 l_1) = 0. \quad (11)$$

Considering the dead-end boundary at the side branch, the impedance can be given by (Chaudhry 1987),

$$Z_{DESB} = \frac{i\sin(\mu_3 l_3)}{Y_3 \cos(\mu_3 l_3)}. \quad (12)$$

Substituting Eq. (12) into Eq. (11) gives,

$$\begin{bmatrix} Y_2 Y_1 \sin(\mu_3 l_3)\cos(\mu_2 l_2)\sin(\mu_1 l_1) \\ -Y_3 Y_2 \cos(\mu_3 l_3)\cos(\mu_2 l_2)\cos(\mu_1 l_1) \\ +Y_3 Y_1 \cos(\mu_3 l_3)\sin(\mu_2 l_2)\sin(\mu_1 l_1) \end{bmatrix} = 0, \quad (13)$$

or in terms of pipe parameters (*D*, *l*, and *a*),

$$\begin{bmatrix} C_{R2}C_{R1}A_3 a_2 a_1 \sin\left(C_{R3}\frac{l_3}{a_3}\omega_{rfb}\right)\cos\left(C_{R2}\frac{l_2}{a_2}\omega_{rfb}\right)\sin\left(C_{R1}\frac{l_1}{a_1}\omega_{rfb}\right) \\ -C_{R3}C_{R2}a_3 a_2 A_1 \cos\left(C_{R3}\frac{l_3}{a_3}\omega_{rfb}\right)\cos\left(C_{R2}\frac{l_2}{a_2}\omega_{rfb}\right)\cos\left(C_{R1}\frac{l_1}{a_1}\omega_{rfb}\right) \\ +C_{R3}C_{R1}a_3 A_2 a_1 \cos\left(C_{R3}\frac{l_3}{a_3}\omega_{rfb}\right)\sin\left(C_{R2}\frac{l_2}{a_2}\omega_{rfb}\right)\sin\left(C_{R1}\frac{l_1}{a_1}\omega_{rfb}\right) \end{bmatrix} = 0. \quad (14)$$

Eq. (13) and Eq. (14) can be further simplified by neglecting the friction effect, i.e., C_R =1. Therefore,

$$Y = -\frac{a}{gA};\ \mu = \frac{\omega}{a}. \quad (15)$$

Furthermore, considering the single main pipeline case, gives,

400 $$A_1 = A_2 = A_0;\ a_1 = a_2 = a_0;\ \text{and}\ Y_1 = Y_2 = Y_0. \tag{16}$$

401 Under the conditions of Eq. (15) and Eq. (16), Eq. (13) can be simplified as,

402 $$\begin{bmatrix} (2+\varepsilon)\cos\left[(\lambda_1+\lambda_2+\lambda_3)\omega_{rfb}\right] \\ -\varepsilon\cos\left[(\lambda_1-\lambda_2-\lambda_3)\omega_{rfb}\right] \\ +(2-\varepsilon)\cos\left[(\lambda_1+\lambda_2-\lambda_3)\omega_{rfb}\right] \\ +\varepsilon\cos\left[(\lambda_1-\lambda_2+\lambda_3)\omega_{rfb}\right] \end{bmatrix} = 0, \tag{17}$$

403 where $\varepsilon = \dfrac{Y_0}{Y_3} = \dfrac{a_0}{a_3}\dfrac{A_3}{A_0}$; and $\lambda = \dfrac{l}{a}$.

404 It is easy to obtain the resonance condition for original intact case of single main pipeline

405 system, ω_{rf0}, given by

406 $$\cos\left[(\lambda_1+\lambda_2)\omega_{rf0}\right] = 0. \tag{18}$$

407 That is,

408 $$\cos\left[\left(\frac{l_1+l_2}{a_0}\right)\omega_{rf0}\right] = \cos\left[\frac{l_0}{a_0}\omega_{rf0}\right] = 0. \tag{19}$$

409 By setting $\omega_{rfb} = \omega_{rf0} + \Delta\omega_{rf}$ or $\Delta\omega_{rf} = \omega_{rfb} - \omega_{rf0}$ where $\Delta\omega_{rf} = \Delta\omega_{rf}(k)$ is the shift (difference) of

410 resonant frequency between the systems with and without side branches for a particular resonant

411 peak (k), the co-sinusoidal functions in Eq. (17) can be expanded about ω_{rf0} with a first-order

412 approximation as (Duan et al. 2013),

413 $$\cos\left[\alpha\omega_{rfb}\right] = \cos\left[\alpha\omega_{rf0}\right] - \alpha\sin\left[\alpha\omega_{rf0}\right]\Delta\omega_{rf} + O\left[(\Delta\omega_{rf})^2\right] + \cdots, \tag{20}$$

414 where α represents the coefficients of the resonant frequency terms in Eq. (17). Note that the

415 resonant peak number has been ignored in Eq. (20) for convenience. Combining Eq. (17) through

416 Eq. (20), gives,

417 $$\Delta\omega_{rf} = \frac{C_u}{C_d}, \tag{21}$$

where,

$$C_u = \begin{bmatrix} (2+\varepsilon)\sin\left[\lambda_3\omega_{rf0}\right] \\ \varepsilon\sin\left[(2\lambda_2+\lambda_3)\omega_{rf0}\right] \\ -(2-\varepsilon)\sin\left[\lambda_3\omega_{rf0}\right] \\ -\varepsilon\sin\left[(2\lambda_2-\lambda_3)\omega_{rf0}\right] \end{bmatrix};\quad C_d = \begin{bmatrix} -(2+\varepsilon)(\lambda_1+\lambda_2+\lambda_3)\cos\left[\lambda_3\omega_{rf0}\right] \\ +\varepsilon(\lambda_1-\lambda_2-\lambda_3)\cos\left[(2\lambda_2+\lambda_3)\omega_{rf0}\right] \\ -(2-\varepsilon)(\lambda_1+\lambda_2-\lambda_3)\cos\left[\lambda_3\omega_{rf0}\right] \\ -\varepsilon(\lambda_1-\lambda_2+\lambda_3)\cos\left[(2\lambda_2-\lambda_3)\omega_{rf0}\right] \end{bmatrix}. \tag{22}$$

Particularly, for relative small side branch, it has,

$$\varepsilon = \frac{Y_0}{Y_3} = \frac{a_0}{a_3}\frac{A_3}{A_0} << 1, \text{ and } \frac{\lambda_3}{\lambda_1+\lambda_2} << 1. \tag{23}$$

As a result, Eq. (21) becomes,

$$\Delta\omega_{rf} = -\frac{\varepsilon}{\lambda_0}\frac{\sin\left[\lambda_3\omega_{rf0}\right]\cos^2\left[\lambda_2\omega_{rf0}\right]}{\cos\left[\lambda_3\omega_{rf0}\right]}, \tag{24}$$

or in dimensionless form,

$$\frac{\Delta\omega_{rf}}{\omega_{th0}} = -\frac{2\varepsilon}{\pi}\frac{\sin\left[\lambda_3\omega_{rf0}\right]\cos^2\left[\lambda_2\omega_{rf0}\right]}{\cos\left[\lambda_3\omega_{rf0}\right]}, \tag{25}$$

where ω_{th0} = theoretical (first resonance) frequency of the intact (DESB-free) pipeline system and $\omega_{th0} = 2\pi\frac{a_0}{4l_0} = \frac{\pi}{2\lambda_0}$ in this study.

References

AL-Khomairi, A. (2008). Leak detection in long pipelines using the least squares method. *J. Hydraulic Res.* 46(3), 392-401.

Beck, S., Curren, M., Sims, N. and Stanway, R. (2005) Pipe network features and leak detection by cross-correlation analysis of reflected waves. *J. Hydraulic Eng.* 131(8), 715 – 723.

Brunone, B. (1999). A transient test-based technique for leak detection in outfall pipes. *J. of Water Resources Planning and Management*, ASCE, 125(5), 302-306.

436 Carter, J.T., Lee, Y., and Buchberger, S.G. (1997). Correlations between travel time and water
437 quality in a deadend loop. *Proc. Wat. Qual. Technol. Conf. Am. Wat. Wks Assoc.*, November
438 9–12, Denver, Co, USA.
439 Chaudhry, M.H. (1987). *Applied hydraulic transients*, 2nd ed. Van Nostrand Reinhold, New York.
440 Colombo, A.F., Lee, P.J., Karney, B.W. (2009). A selective literature review of transient-based
441 leak detection methods. *J. Hydro-environment Research*, IAHR, 2(4), 212-227.
442 Covas, D., Ramos, H., Almeida, A.B. (2005). Standing wave difference method for leak
443 detection in pipeline systems. *J. Hydraulic Eng.* 131(12), 1106-1116.
444 Duan, H.F., Tung, Y.K., Ghidaoui, M.S., (2010a). Probabilistic analysis of transient design for
445 water supply systems. *J. of Water Resources Planning and Management*, ASCE, 136(6),
446 678-687.
447 Duan, H.F., Lee, P.J., Ghidaoui, M.S., Tung, Y.K. (2010b). Essential system response
448 information for transient-based leak detection methods. *J. of Hydraulic Research*, IAHR,
449 48(5), 650-657.
450 Duan, H.F., Lee, P.J., Ghidaoui, M.S., and Tung, Y.K. (2011). Leak detection in complex series
451 pipelines by using system frequency response method. *J. of Hydraulic Research*, IAHR, 49(2),
452 213-221.
453 Duan H.F., Lee P.J., Ghidaoui M.S., and Tung Y.K. (2012a). Extended blockage detection in
454 pipelines by using the system frequency response analysis. *J. of Water Resources Planning*
455 *and Management*, ASCE, 138(1), 55-62.
456 Duan, H.F., Lee, P.J., Ghidaoui, M.S., and Tung, Y.K. (2012b). System response function based
457 leak detection in viscoelastic pipeline. *J. of Hydraulic Engineering*, ASCE, 138(2), 143-153.
458 Duan, H.F., Lee, P.J., Kashima, A., Lu, JL, Ghidaoui, M.S., and Tung, Y.K. (2013). Extended
459 blockage detection in pipes using the frequency response method: analytical analysis and experimental
460 verification. *J. of Hydraulic Engineering*, ASCE, 139(7), 763-771.

461 Duan, H.F., Lee, P.J., Ghidaoui, M.S., and Tuck, J. (2014). Transient wave-blockage interaction
462 and extended blockage detection in elastic water pipelines. *J. Fluids Structures*, 46 (2014), pp.
463 2-16.
464 Ferrante, M., Brunone, B., and Meniconi, S. (2007). Wavelets for the analysis of transient
465 pressure signals for leak detection. *J. of Hydraulic Engineering,* ASCE, 133(11), 1274-1282.
466 Ferrante, M., Brunone, B., and Meniconi, S. (2009). Leak detection in branched pipe systems
467 coupling wavelet analysis and a Lagrangian model. *J Water Supply Res Technol* AQUA 58(2):
468 95-106.
469 Ghidaoui M.S., Zhao M., McInnis D.A., and Axworthy D.H. (2005). A review of waterhammer
470 theory and practice. *Appl. Mech. Reviews*, 58, pp. 49-76.
471
472 Karney, B.W., and McInnis, D. (1990). Transient analysis of water distribution systems. *J. of the*
473 *American Water Works Association (AWWA),* 82(7), 62-70.
474 Kim, S.H. (2008). Address-oriented impedance matrix method for generic calibration of
475 heterogeneous pipe network systems. *J. of Hydraulic Engineering*, ASCE, 134(1), 66-75.
476 Kim, S.H., Zecchin, A., and Choi, L. (2014). diagnosis of a pipeline system for transient flow in
477 low reynolds number with impedance method. *J. of Hydraulic Engineering*, ASCE, DOI:
478 10.1061/(ASCE) HY,1943-7900.0000945.
479 Lee, P.J., Lambert, M.F., Simpson, A.R., Vítkovský, J.P., and Liggett J. (2006). Experimental
480 verification of the frequency response method for pipeline leak detection. *J. of Hydraulic*
481 *Research*, IAHR, 44(5), 693-707.
482 Lee, P.J., Vítkovský, J.P., Lambert, M.F., Simpson, A.R., and Liggett J. (2008). Discrete
483 blockage detection in pipelines using the frequency response diagram: numerical study. *J. of*

484 *Hydraulic Engineering*, ASCE, 134(5), 658-663.
485 Lee, P.J., and Vítkovský, J.P. (2010) Quantifying linearization error when modeling fluid
486 pipeline transients using the frequency response method. *J. of Hydraulic Engineering*, ASCE,
487 136(10), 831-836.
488 Lee, P.J., Duan, H.F., Tuck, J., and Ghidaoui, M.S., (2014). Numerical and experimental
489 illustration of the effect of signal bandwidth on pipe condition assessment using fluid
490 transients. *J. of Hydraulic Engineering*, ASCE, DOI:10.1061/(ASCE)HY.1943-
491 7900.0000961, 04014074.
492 Liggett, J.A., Chen, L.C. (1994). Inverse transient analysis in pipe networks. *J. of Hydraulic*
493 *Engineering*, ASCE, 120(8), pp. 934-954.
494 Meniconi, S., Brunone, B., Ferrante, M., and Massari, C. (2011a). Transient tests for locating and
495 sizing illegal branches in pipe systems. *J. of Hydro-informatics*, 13(3), 334-345.
496 Meniconi, S., Brunone, B., Ferrante, M., and Massari, C. (2011b). Small amplitude sharp
497 pressure waves to diagnose pipe systems. *Water Resources Management* 25, 79-96.
498 Meniconi, S., Brunone, B., and Ferrante, M. (2011c). In-line pipe device checking by short
499 period analysis of transient tests. *J. of Hydraulic Engineering*, ASCE, 137(7), 713-722.
500 Meniconi, S., Duan, H.F., Lee, P.J., Brunone, B., Ghidaoui, M.S., and Ferrante, M. (2013).
501 Innovative transient analysis approach vs. laboratory tests for partial blockage detection in
502 plastic and metallic pipelines. *J. of Hydraulic Engineering*, ASCE, 139(10), 1033-1040.
503 Mohapatra, P.K., Chaudhry, M.H., Kassem, A.A., and Moloo, J. (2006). Detection of partial
504 blockage in single pipelines. *J. of Hydraulic Engineering*, ASCE, 132(2), 200-206.
505 Sattar, A.M., Chaudhry, M.H., and Kassem, A.A. (2008). Partial blockage detection in pipelines
506 by frequency response method. *J. of Hydraulic Engineering*, ASCE, 134(1), 76-89.

507 Stephens, M.L. (2008). Transient response analysis for fault detection and pipeline wall
508 condition assessment in field water transmission and distribution pipelines and networks. *PhD*
509 *Thesis*, The University of Adelaide, SA, Australia.
510 Tuck, J., Lee, P., Davidson, M., and Ghidaoui, M. (2013). Analysis of transient signals in
511 pipeline systems with extended blockages. *Journal of Hydraulic Research*, IAHR, 51(6), 623-
512 633.
513 Vardy, A. and Brown, J. (1995). Transient, turbulent, smooth pipe friction. *J. Hydraulic Res.*,
514 IAHR, 33(4), 435 – 456.
515 Vítkovský, J.P., Simpson, A.R., and Lambert M.F. (2000). Leak detection and calibration using
516 transients and genetic algorithms. *J. Water Res. Planning and Management*, ASCE, 126(4),
517 pp. 262-265.
518 Vítkovský, J. P., Lambert, M. F., Simpson, A. R., and Bergant, A. (2003). "Frequency-domain
519 transient pipe flow solution including unsteady friction." *Proc., Int. Conf. on Pumps,*
520 *Electromechanical Devices and Systems Applied to Urban Water Management*, Vol. 2, E.
521 Cabrera and E. Cabrera, Jr., eds., Swets and Zietlinger Publishers, Netherlands, 773–780.
522 Vítkovský, J.P., Lambert, M.F., Simpson, A.R., Liggett, J.A. (2007). Experimental observation
523 and analysis of inverse transients for pipeline leak detection. *J. Water Res. Planning and*
524 *Management* 133(6), 519-530.
525 Walski, T.M., Chase, D.V., Savic, D.A., Grayman, W., Beckwith, S., and Koelle, E. (2003).
526 *Advanced Water Distribution Modeling and Management*, Bentley Institute Press, USA.
527 Wang, X.J., Lambert, M.F., Simpson, A.R., Liggett, J.A., Vítkovský, J.P. (2002). Leak detection
528 in pipeline systems using the damping of fluid transients. *J. of Hydraulic Engineering*, ASCE,
529 128(7), 697-711.

Wang, X.J., Lambert, M.F., and Simpson, A.R. (2005a). Detection and location of a partial blockage in a pipeline using damping of fluid transients. *J. of Water Resources Planning and Management*, ASCE, 131(3), 244-249.

Wang, X.J., Lambert, M.F., and Simpson, A.R. (2005b). Behavior of short lateral dead ends on pipe transients: a lumped parameter model and an analytical solution. *J. of Fluids Engineering* ASME, 127(5), 529-535.

Wylie E.B., Streeter V.L., and Suo L. (1993). *Fluid transients in systems*. Prentice Hall, Inc. Englewood Cliffs, New Jersey.

Zielke, W. (1968). Frequency-dependent friction in transient pipe flow. *J. Basic Eng.*, ASME, 90(1), pp. 109-115.

Listing of figure captions

Fig. 1: Illustrative pipe system with single dead-end side branch (pipe section no. 3)

Fig. 2: Comparison of transient responses for system with and without dead-end side branch: (a) time domain results; (b) frequency domain results

Fig. 3: Flowchart of GA-based optimization for dead-end side branch detection

Fig. 4: Flow perturbations of side-discharge valve at downstream end

Fig. 5: Simulated pressure head traces at downstream valve in the pipe system with and without side branch: (a) time domain results; (b) frequency domain results

Fig. 6: GA-based optimization process of DESB detection for test no. 1

Fig. 7: Resonant frequency shifts by optimization process and 1D model simulation

Fig. 8: Input signals for different side-dischange valve operations

576

577

578

579 **Listing of table captions**

580 **Table 1:** System settings for numerical tests

581 **Table 2:** Side branch detection results for all numerical tests

582 **Table 3:** Detection results for test no. 1 by different input signals

583

Tables
Click here to download Table: TablesR.docx

Table 1. System settings for numerical tests

Test no.	Section no. 1			Section no. 2			Section no. 3 (DESB)			Initial Reynolds number ($\boldsymbol{Re}_0$) ($\times 10^3$)
	l_1 (m)	D_1 (mm)	a_1 (m/s)	l_2 (m)	D_2 (mm)	a_2 (m/s)	l_3 (m)	D_3 (mm)	a_3 (m/s)	
1	350	500	1000	650	500	1000	50	100	1200	1
2	350	500	1000	650	500	1000	50	100	1200	5
3	350	500	1000	650	500	1000	50	100	1200	10
4	300	500	1000	700	400	1100	50	200	1200	5
5	350	500	1000	650	500	1100	50	200	1200	10
6	350	500	1000	650	400	1100	150	300	1200	10
7	550	500	1000	450	400	1100	50	100	1200	30
8	550	500	1000	450	400	1100	50	50	1200	30
9	700	500	1000	300	400	1000	50	50	1300	100
10	550	500	1000	450	400	1100	50	50	1300	100

Table 2. Side branch detection results for all numerical tests

Test no.	D_3 (mm)			l_3 (m)			a_3 (m/s)			l_2 (m)		
	$D_{3,r}$	$D_{3,p}$	γ (%)	$l_{3,r}$	$l_{3,p}$	γ (%)	$a_{3,r}$	$a_{3,p}$	γ (%)	$l_{2,r}$	$l_{2,p}$	γ (%)
1	100	103	3.0	50	51	2.0	1200	1210	0.8	650	650	0.0
2	100	102	2.0	50	50	0.0	1200	1199	0.1	650	661	1.7
3	100	100	0.0	50	51	2.0	1200	1193	0.6	650	653	0.5
4	200	211	5.5	50	47	6.0	1200	1219	1.6	700	707	1.0
5	200	205	2.5	50	54	8.0	1200	1189	0.9	650	650	0.0
6	300	256	**14.7**	150	135	10.0	1200	1243	3.6	650	674	**3.7**
7	100	113	13.0	50	57	**14.0**	1200	1145	**4.6**	450	445	1.1
8	100	106	6.0	150	139	7.3	1200	1235	2.9	450	456	1.3
9	50	52	4.0	50	56	12.0	1300	1291	0.7	300	308	2.7
10	50	54	8.0	50	54	8.0	1300	1281	1.5	450	443	1.6

Table 3. Detection results for test no. 1 by different input signals

Signal no.	D_3 (mm)			l_3 (m)			a_3 (m/s)			l_2 (m)		
	$D_{3,r}$	$D_{3,p}$	γ (%)	$l_{3,r}$	$l_{3,p}$	γ (%)	$a_{3,r}$	$a_{3,p}$	γ (%)	$l_{2,r}$	$l_{2,p}$	γ (%)
#1	100	103	2.9	50	51	2.0	1200	1210	0.8	650	650	0.0
#2	100	92	8.7	50	54	**7.4**	1200	1211	**0.9**	650	650	0.0
#3	100	115	**13.0**	50	47	6.4	1200	1206	0.5	650	653	**0.5**

Figure 1
Click here to download Figure: Fig 1.pdf

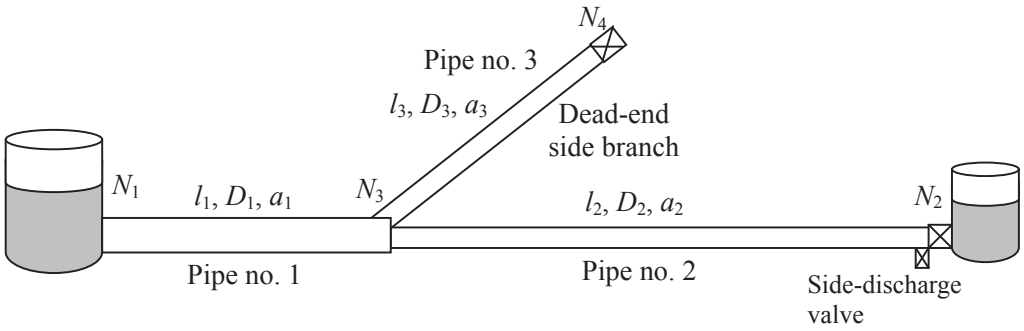

Fig. 1. Illustrative pipe system with single dead-end side branch (pipe section no. 3)

Figure 2
Click here to download Figure: Fig 2.pdf

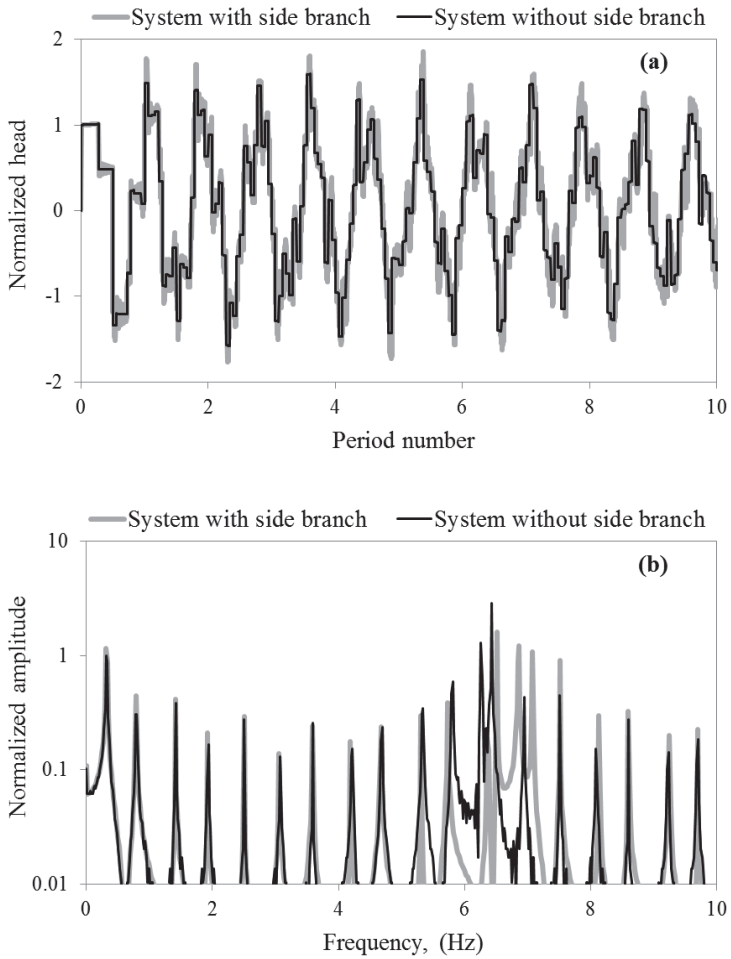

Fig. 2. Comparison of transient responses for system with and without dead-end side branch: (a) time domain results; (b) frequency domain results

Figure 3
Click here to download Figure: Fig 3.pdf

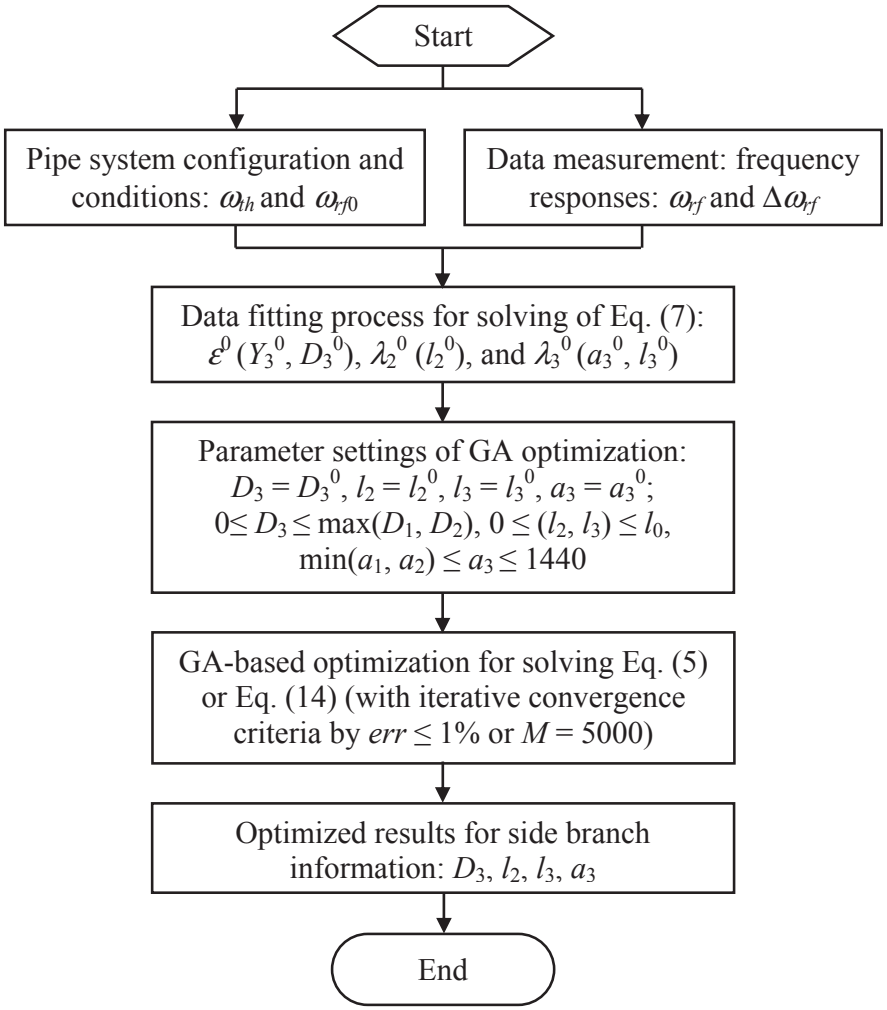

Fig. 3. Flowchart of GA-based optimization for dead-end side branch detection

Figure 4
Click here to download Figure: Fig 4.pdf

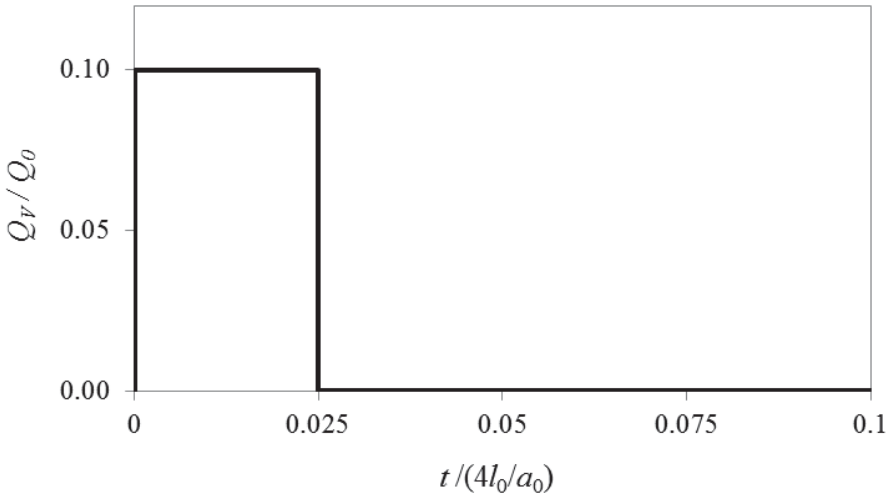

Fig. 4. Flow perturbations of side-discharge valve at downstream end

Figure 5
Click here to download Figure: Fig 5.pdf

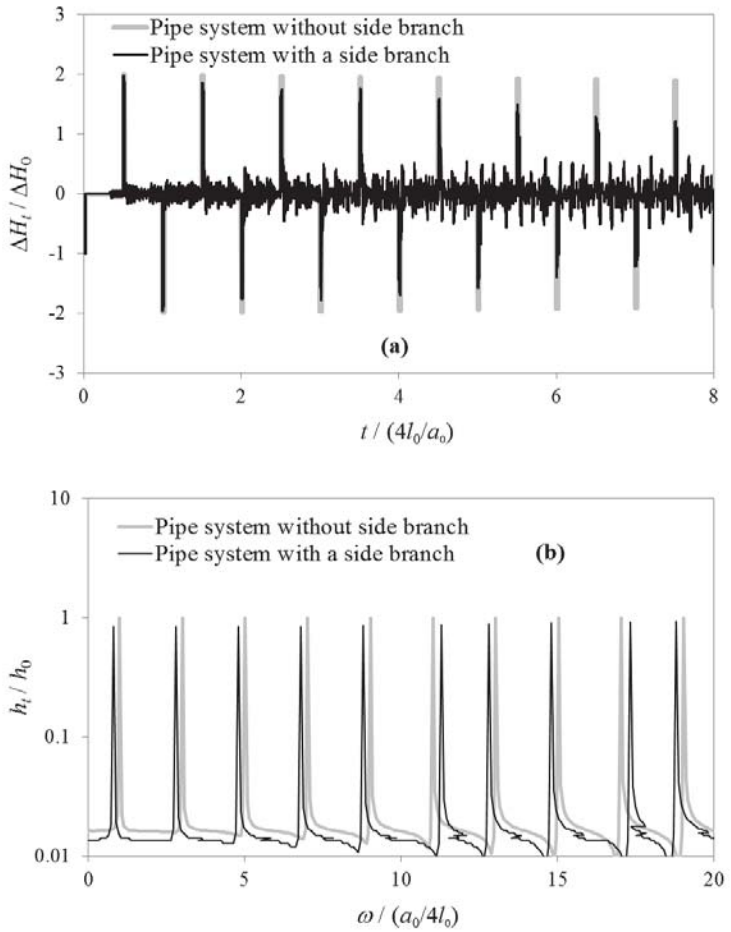

Fig. 5. Simulated pressure head traces at downstream valve in the pipe system with and without side branch: (a) time domain results; (b) frequency domain results

Figure 6
Click here to download Figure: Fig 6.pdf

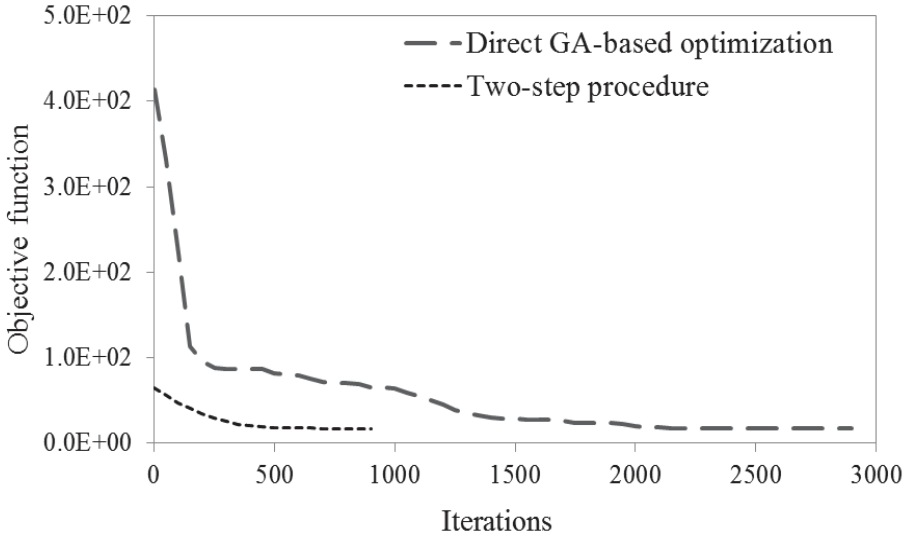

Fig. 6. GA-based optimization process of DESB detection for test no. 1

Figure 7
Click here to download Figure: Fig 7.pdf

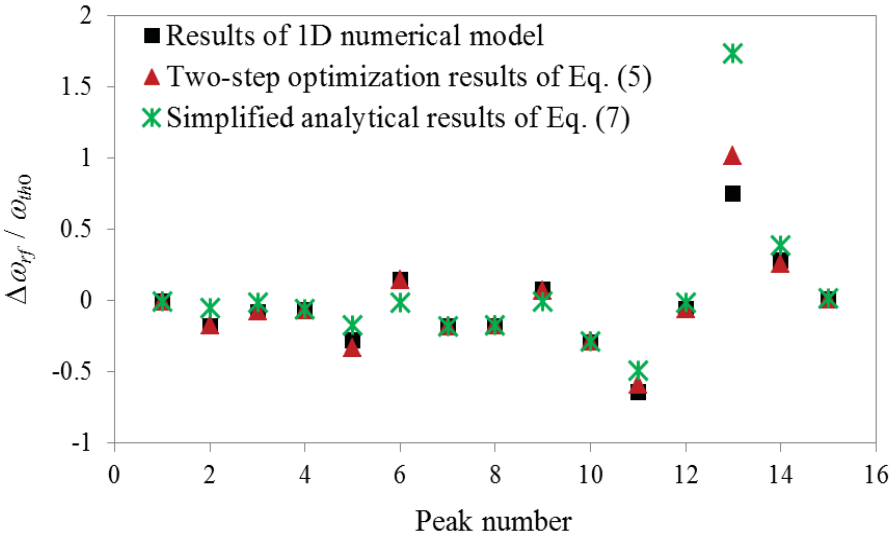

Fig. 7. Resonant frequency shifts by optimization process and 1D model simulation

Figure 8
Click here to download Figure: Fig 8.pdf

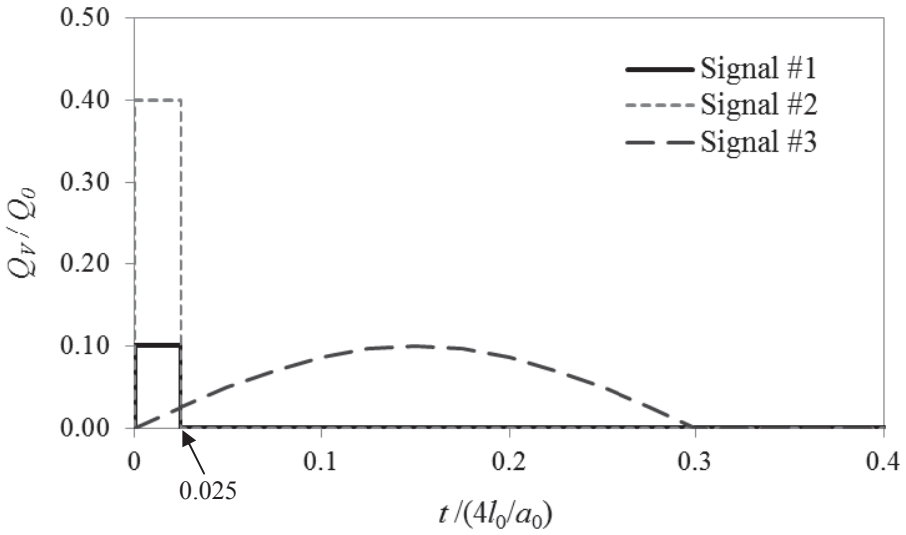

Fig. 8. Input signals for different side-dischange valve operations